Journal of Drug Delivery Science and Technology 108 (2025) 106809

Contents lists available at ScienceDirect

Journal of Drug Delivery Science and Technology

journal homepage: www.elsevier.com/locate/jddst

The influence of adsorption incorporation mechanism on the release of isoniazid by montmorillonite

Jessica de Carvalho Arjona [a,b], Carina Ulsen [c], Dayane Tada [d], Francisco Rolando Valenzuela Diaz [a], Nicole Raymonde Demarquette [b,*]

[a] Departamento de Engenharia Metalúrgica e de Materiais, Escola Politécnica, Universidade de São Paulo, São Paulo, 05508-030, Brazil
[b] Mechanical Engineering Department, École de Technologie Supérieure, Montréal, QC, H3C 1K3, Canada
[c] Departamento de Engenharia de Minas e de Petróleo, Escola Politécnica, Universidade de São Paulo, São Paulo, 05508-030, Brazil
[d] Universidade Federal de São Paulo, Laboratory of Nanomaterials and Nanotoxicology, Rua Talim, 300 São José dos Campos, São Paulo, Brazil

ARTICLE INFO

Keywords:
Isoniazid
Montmorillonite
Drug controlled release
pH dependence drug release
Adsorption

ABSTRACT

Studies on the use of clay as a drug delivery vehicle have increased in recent years. Its applicability in the pharmaceutical field offers a low-cost solution to addressing drug side effects. Among the drugs that may benefit from a controlled release system is isoniazid (INH), a medication used in tuberculosis treatment. However, to enhance the clay-drug loading capacity and improve sustained drug release, the interaction between clay and drug must be thoroughly understood. This study used montmorillonite (Mtt) to develop Mtt-INH hybrids. Adsorption mechanisms were investigated under two pH conditions. At pH 7, where the drug is in its neutral state, two adsorption phases: the formation of a monolayer (20 mg/g) hybrid (a), followed by multilayer adsorption which can exceed 50 mg/g, hybrid (b) were achieved. At pH 2, where the drug protonates and carries a positive charge, the highest loading capacity of 100 mg/g, (hybrid (c) was achieved at the lowest drug concentration. Different from previous studies, the INH release profile was influenced by the amount adsorbed and the clay-drug interactions. For the hybrids (a) and (c), which correspond to monolayer adsorption, the release profile in intestine pH conditions closely followed the Zero Order Model, ($R^2 > 0.93$). These hybrids exhibited slower release rates than hybrid (b) consistent with their stronger clay-drug interactions observed during adsorption. *In vitro* cytocompatibility assays demonstrated that neither pristine clay nor hybrid (c) was cytotoxic to fibroblast cells, supporting the potential of Mtt-based systems for pharmaceutical applications. The results may guide future studies to optimize controlled drug release by considering the expected application and the interactions between the clay-drug system and the pH during the adsorption process.

1. Introduction

The use of clays in pharmaceutical and medical fields has been studied for decades [1]. Initially, clays were extensively utilized as tablet excipients and in creams and ointments [2]. During these applications, it was observed that the drug release profile varied depending on the type of clay used as an excipient. Notably, some medications exhibited extended or delayed release profiles, prompting further studies to understand the potential interactions between clay and drug [2,3]. These interactions are influenced not only by the clay's morphology, microstructure, chemical composition, and surface charge, as well as the chemical structure and ionization state of the drug [4].

Among the various clays used in pharmaceutical applications, montmorillonite (Mtt) is one of the most common and widely utilized due to its swelling and sorption properties. Mtt consists of lamellas stacked and held together by van der waals forces with exchangeable cations neutralizing the negative surface charge resulted from isomorphic substitutions in the crystal structure [5–7]. While numerous studies have investigated the use of Mtt in drug release systems, only a limited number have analyzed the adsorption and release mechanisms considering the influence of the environmental pH during these processes. Drugs studied for these applications include antipsychotics [8], anticancer agents [9–12], antibiotics [10,13–15], anti-inflammatory drugs [16,17], anthelmintics [18], vitamins [19], anxiolytics [20], and treatments for glaucoma [21]. The major goal of developing controlled-release systems for these medications is to reduce side effects

* Corresponding author.
E-mail address: nicoler.demarquette@etsmtl.ca (N.R. Demarquette).

https://doi.org/10.1016/j.jddst.2025.106809
Received 5 February 2025; Accepted 12 March 2025
Available online 15 March 2025

and enhance the efficiency of drug treatment. As shown in previous studies, the pH of the environment plays a crucial role in drug adsorption due to its impact on the drug pKa. Depending on its chemical structure, the drug's charge can vary with pH, significantly altering its interaction with the clay surface.

Isoniazid (INH), a key drug used in all forms of tuberculosis treatment, has been the focus of increasing research on controlled-release systems in recent years. Prolonged use of INH is known to cause side effects, such as liver and kidney failure, highlighting the need for innovative delivery systems. In addition to polymeric systems [22–26], inorganic particles have attracted attention due to their low cost and stability. Examples include silica nanoparticles [27], palygorskite [28–30], halloysite [31,32], sepiolite [30], layered double hydroxides (LDH) [33,34], saponite [35], zeolites [36,37], hectorite [38], and montmorillonite (Mtt) [35,38–40]. These studies have explored various aspects of INH incorporation. Some focused on understanding the interaction between clay and INH [30,35], while others examined incorporation without analyzing the release profile [29,31,34,37,39,40]. Only a few studies investigated INH incorporation concerning pH environment [27,28]. Souza et al. (2021) [36] reported the adsorption isotherm pH 3 for zeolites but did not compare it with other pH conditions. Such comparisons are crucial to understanding clay-drug interactions, as the pKa values of INH, (2.0, 3.6, and 10.8) influence its chemical structure and interaction with clay surface depending on the environment pH. Based on the drug's pKa, we confirm that it remains neutral at pH 7 and becomes cationic at pH 3.6. However, at pH 2, protonation occurs at the hydrazine group and the pyridine ring, potentially enhancing interactions with the negatively charged surface. This can increase the adsorption capacity while giving a more sustained release by clays.

In this study, we investigate the adsorption and release behavior of INH on Mtt, focusing on the impact of pH during adsorption (pH 2 and 7) and the resulting drug-clay interactions. Adsorption behavior was analyzed using Gile's adsorption isotherm theory, which provides insights into the nature of adsorbate-absorbent interactions based on the shape of the adsorption curve [41,42]. To characterize the resulting hybrids, various techniques were employed, FTIR to identify chemical interaction between the drug and the clay, XRD to determine whether the drug was located on the clay surface or between lamellas, TGA to confirm the presence of INH post-adsorption, and DSC to evaluate the effect of Mtt on the thermal transformation of INH transformation. Additionally, an *in vitro* cell viability assay was conducted for both pristine Mtt and Mtt/INH hybrid as a preliminary test to assess the potential use of this clay for biomedical applications.

2. Materials and methods

2.1. Materials

Isoniazid, $NaHPO_4$, NaCl, NaOH, and HCl 37 % solution were standard reagents from Sigma Aldrich, all materials were used as received. A purified Brazilian Northeast smectite from Vitoria da Conquista, Bahia, Brazil, was used. The clay was stirred in water (15 % w/w) at 14,000 rpm for 20 min to form an aqueous dispersion and left to rest. After resting, the dispersion was spread into three phases with different colors, which were carefully separated [38,43]. The first decanted phase, a green clay, denominated Mtt, was used in this work. Table 1 shows the chemical composition of Mtt, further details about mineral composition and porosity can be found in previous papers [38,43].

2.2. Methodology

2.2.1. Clay drug adsorption isotherms

The INH adsorption tests by clay were conducted using 0.1 g of clay into dialysis tubing cellulose membrane (14,000 Da) at pH 2 and 7. For each pH, 14 solutions were prepared with INH concentrations ranging from 68.5 to 5480.0 mg/L (0.5–40 mmol/L). Mtt was added to each solution at a concentration of 10 g/L followed by magnetic stirring for 3 h [38]. The remaining INH in the solution was quantified using a Thermo Scientific Evolution 260 Bio UV–visible spectrophotometer (UV–vis) with distinct calibration curves prepared for each pH condition. At the end of the experiment, a curve of q_{ab} (amount of INH that was adsorbed by clay, in mg/g) as a function of C_e (concentration in equilibrium after the adsorption in mg/L) was plotted and fitted to mathematical models to elucidate the adsorption mechanism. From the resulting adsorption curves, three Mtt-INH hybrids (a), (b), and (c) were selected for further experiments. Hybrids (a) and (b), prepared at pH 7, correspond to the monolayer and multi-layer adsorption, respectively. Hybrid (c), obtained at pH 2, represents monolayer adsorption.

2.2.2. Mtt and Mtt-INH hybrids' characterization

Fourier transformation Infrared spectroscopy (FTIR) spectra were obtained using a PerkinElmer Spectrum Two FT-IR spectrometer in the wavenumber range of 4000 cm^{-1} to 600 cm^{-1} with 4 cm^{-1} of resolution. FTIR is an important characterization technique, as band shifts indicate changes in the vibrational modes of certain bonds due to interactions between clay and INH. X-ray diffraction (XRD) patterns were recorded using a Malvern Panalytical Empyrean DY-2516 X-ray diffractometer equipped with kCu_α radiation, scanning over a 2θ range of 3°–30° at 1°/min. Thermal gravimetric analysis (TGA) was conducted using a Pyris Diamond TG/DTA PerkinElmer thermogravimetric analyzer. Mass loss was evaluated for pristine clay and its respective hybrids under an airflow of 100 mL/min, over a temperature range of 40–800 °C for clays and clay/INH hybrids, and 40–600 °C for pure INH, at a heating rate of 10 °C/min. Differential scanning calorimetry (DSC) measurements were performed using a DSC 2500 TA Discovery Series under a nitrogen atmosphere with a 50 mL/min gas flow. Samples were heated in hermetic aluminum pans from 40 °C to 230 °C at a heating rate of 10 °C/min.

2.2.3. Kinetic drug release test

The kinetic drug release test was conducted for hybrids Mtt-INH hybrids (a), (b), and (c) to investigate the influence of different incorporation mechanisms: monolayer adsorption, multilayer incorporation, and monolayer adsorption at pH 2, respectively. The release simulated oral drug administration by immersing the hybrids in buffer solutions with pH 2, pH 6.8, and pH 7.4, corresponding to the stomach and first and second zones of the small intestine. The release was monitored over 8 h (480 min); with samples collected every 30 min to measure the amount of INH released. All experiments were performed in triplicate to ensure reproducibility. The resulting release data were fitted to three release models: Zero order, Korsmeyer-Peppas, and Higuchi.

2.2.4. Cytotoxicity in vitro assays

In vitro assays were conducted to evaluate the cytotoxicity of the Mtt and the hybrid Mtt/INH (c). Cytotoxicity was assessed against L929 fibroblast cells using the indirect method, following the ISO-10993-2009 protocol. Sample extracts were prepared in Dulbeccos' Modified Eagle Medium (DMEM) supplemented with 10 % fetal bovine serum (FBS). The samples were suspended in the culture medium at 0.2 g/mL concentration as recommended in ISO-10993-2007 for irregular powder

Table 1
Chemical composition of Mtt.

Analyte		SiO_2	Al_2O_3	Fe_2O_3	MnO	MgO	CaO	Na_2O	K_2O	TiO_2	P_2O_5	LOI
Mass	(%)	56.20	21.10	7.94	<0.10	3.60	0.21	<0.10	<0.10	0.75	<0.10	10.30

shape materials. Cell culture medium without samples was maintained under identical conditions and served as the negative control. Cells from the L929 cell line were plated after 80 % confluence at the concentration of 0.25 × 10^4 cells/well in a 96-well cell plate with DMEM supplemented with 10 % FBS (v/v) and with streptomycin (0.1 g/L) and ampicillin (0.025 g/L). The cells were incubated for 24 h, and the cell viability was assessed by the MTT method. After incubation, the medium was removed, and each well was carefully washed with phosphate buffer saline (pH 7). Following, 100 μL of aqueous solution of MTT (3-[4,5-dimethylthiazol-2-yl]-2,5 diphenyl tetrazolium bromide) at 0.5 mg/mL was added in each well. The cells were incubated for 3 h and the MTT solution was replaced by 100 μL of DMSO to solubilize the formazan crystals. After 30 min, the absorbance at 480 nm was measured in a plate reader (Biotek Synergy 2). Cell viability was calculated by considering the average absorbance in the wells where cells were incubated with the negative control of cytotoxicity as 100 % of viability according to the (Eq. (1)). The assay was performed in quintuplicate.

$$\textit{cell viability}\ (\%) = \frac{\textit{Absorbance at 480 nm samples}}{\textit{Average Absorbance 480 nm of negative control}}\ x\ 100 \quad \text{(Eq. 1)}$$

The L929 fibroblast cells were selected for cytotoxicity evaluation due to their well-established use in biocompatibility testing, as recommended by international standards such as ISO 10993 (as used). Their rapid proliferation and consistent response allow for reproducible and comparative cytotoxicity assessments. Additionally, fibroblasts play a role in tissue remodeling and wound healing, which are relevant in the context of tuberculosis-related inflammation and fibrosis. Future studies will incorporate lung-relevant cell models to further evaluate the material's effects in a more disease-specific context.

3. Results

3.1. Adsorption studies

Fig. 1 shows the adsorption curves of isoniazid by Mtt at pH 2 and 7. In the graph, the amount of INH adsorbed (mg/g) is plotted in function of the remaining INH concentration (mg/L) on the solution after the adsorption. The data indicate that the clay's adsorption capacity increases as the pH decreases. At pH 7, the amount of drug adsorbed rises sharply until reaching approximately 20 mg/g, as marked at point (a) in Fig. 1, where the curve appears to plateau. This region corresponds to the monolayer adsorption capacity, a behavior also observed by Carazo et al. (2018) [40]. Beyond this point, the adsorption continues with the deposition of additional drug molecules, forming multilayers as indicated at point (b). At pH 2, the clay fully adsorbed INH at initial solution concentrations below 800 mg/L, in which the higher total adsorption was 80 mg/g. As the INH concentration increased, adsorption continued until a plateau reached around 100 mg/g as shown near point (c) in Fig. 1. The distinct shapes of the adsorption curves at pH 2 and 7 suggest that the adsorption mechanism differs between the two pH conditions [41,42].

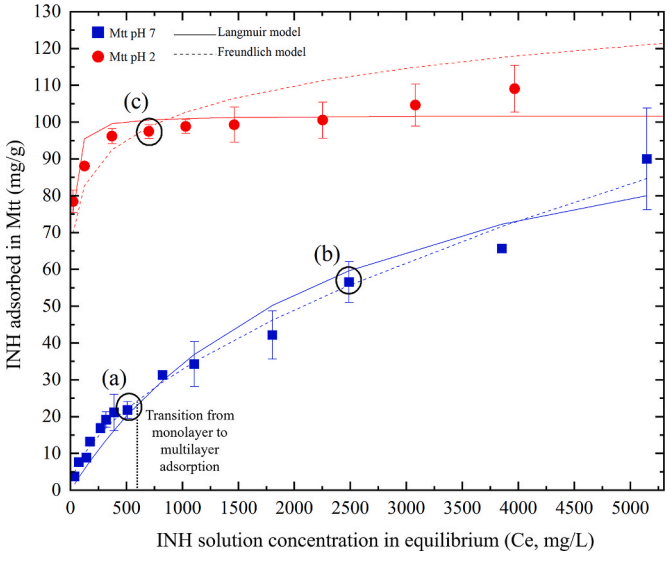

Fig. 1. Adsorption curves of INH by Mtt at pH 2 and pH 7.

The data presented in Fig. 1 were fitted to two mathematical models, Langmuir (Eq. (2)) and Freundlich (Eq. (3)), as described in Table 2. In these equations, C_s and C_e represent the amount of drug adsorbed (mg/g) in the equilibrium drug concentration (mg/L) respectively; Q_M is the theoretical maximum clay adsorption capacity, while K_L and K_F are the Langmuir and Freundlich constants respectively. Table 2 also summarizes the parameters obtained from fitting the adsorption data at pH 2 and 7. The data best fitted by the Freundlich model, with R^2 values of 0.956 and 0.987 for pH 2 and 7, respectively. This suggests that the drug occurred on a heterogeneous surface [44]. This can be attributed to various active sites on the clay structure, including hydroxyl groups at the edges and interlayer spaces, which facilitate non-uniform adsorption. Conversely, at pH 2, the protonation of INH leads to a positively charged species, enhancing electrostatic attraction with the negatively charged clay surface, which likely dominates the adsorption mechanism. For the Langmuir model (Eq. (2)), the Q_M parameter reflects the clay's maximum incorporation capacity. At pH 2, this value was determined to be 101.8 mg/g; at pH 7, it was slightly higher at 117.7 mg/g.

3.2. FTIR

Fig. 2 presents the FTIR spectra of INH, Mtt, and the Mtt-INH hybrids. For Mtt, typical montmorillonite bands were observed: the band at approximately 998 cm^{-1} corresponds to the Si-O vibration [45], near 910 cm^{-1} is attributed to Al-Al-OH deformation. The broad bands around 3600 cm^{-1} are associated with O-H vibration from water molecules [43]. Characteristic INH bands were detected in all Mtt/INH hybrids. The intensity and number of INH bands in the spectra increased with the amount of INH incorporated, as seen in hybrids Mtt-INH (b) and (c). The hybrid with the lowest INH content, Mtt-INH (a) exhibited only an INH band around 1437 cm^{-1}. Additional INH bands were present in Mtt-INH (b) at 1668, 1539, 1502, 1428, and 841 cm^{-1}. For Mtt-INH (c), the hybrid with the highest adsorption, these bands were complemented by additional peaks at 1692 and 1248 cm^{-1}. A shift in the 1632 cm^{-1} band was observed across all hybrids moving to 1630, 1625, and 1622 cm^{-1}, for Mtt/INH (a), (b), and (c), respectively. Additionally, the Si-O vibration band characteristic of Mtt shifted upwards, 998 cm^{-1} to 1003 cm^{-1} in Mtt/INH (c).

3.3. XRD

Fig. 3 shows the XRD patterns of Mtt, its respective hybrids, and INH. The Mtt-INH hybrids did not present the peaks of INH, indicating that

Table 2
Fit model parameters of INH adsorption by Mtt at pH 2 and pH 7.

Model	Equation	Eq.	Parameters	pH	
				2	7
Langmuir	$C_s = \frac{Q_M \bullet K_L \bullet C_e}{1 + K_L \bullet C_e}$	(Eq. (2))	K_L(L/mg)	0.1201	0.0004
			Q_M (mg/g)	101.8349	117.7125
			R_L	0.0756	0.9536
			R^2	**0.7442**	**0.9648**
Freundlich	$C_s = K_F \bullet C_e^n$	(Eq. (3))	K_F	50.4232	0.6115
			N_F	9.7450	1.7330
			R^2	**0.9555**	**0.9873**

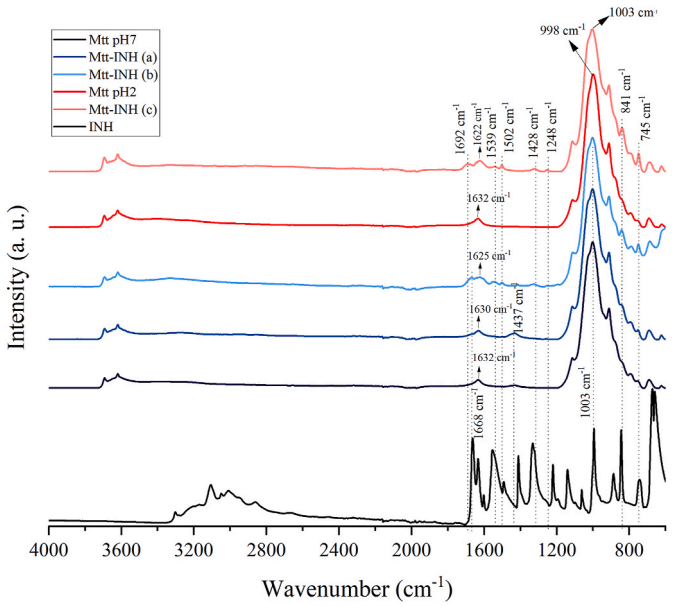

Fig. 2. FTIR spectra of Mtt, Mtt/INH hybrids, and INH.

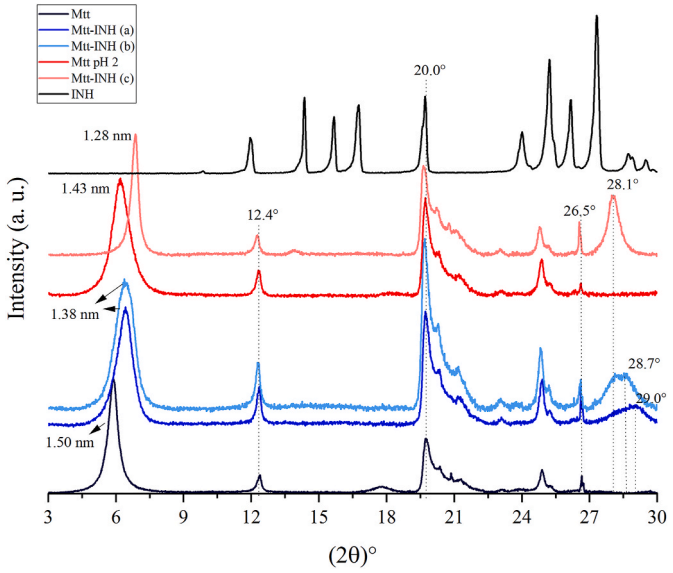

Fig. 3. XRD patterns of Mtt and its hybrids.

the drug was not crystalline on a clay surface, or that the molecules were organized in a particular way their peak intensities decreased. Organoclays, for instance, show an increase in d001 distance only for organic salts with more than 10 carbons on their chain, which could explain why these samples did not exhibit an increase in their interlayer distance [46]. The interlayer spacing did not increase after clay adsorption, instead, it appeared to decrease from 1.50 nm to 1.38 nm for the hybrids made at pH 7, and from 1.43 nm to 1.28 nm, for Mtt-INH (c). Similar results were observed for other drugs [10,11,17]. The intensification of peaks at of 20.0° and 26.5°, along with the appearance of peaks around 28.1°, 28.7°, and 29.0°, also suggests the presence of INH in Mtt crystal [14] may suggest that part of the drug was crystalline on the clay surface.

3.4. TGA

Fig. 4 shows the TGA curves for INH, Mtt, and its hybrids. INH exhibited a one-step thermal degradation, starting at 126 °C and ending at around 350 °C with no residue. Clay and its hybrids displayed a three-stage degradation curve: evaporation of surface water, loss of internal water molecules, and dihydroxylation. Mtt at pH 2 presented a reduction in surface water compared to Mtt due to the incorporation of H^+ on the clay surface in the acidic pH [47]. The amount of INH incorporated influenced the degradation process of hybrids. For all hybrids, the increase in the amount of INH absorbed resulted in a decrease in the surface water loss. The presence of INH in Mtt-INH hybrids also increased the third stage of the clay degradation suggesting that the drug degraded at a temperature above 300 °C.

Table 3 presents the temperature and weight loss percentages for Mtt and its hybrids. As seen, in the first stage of degradation, the temperature range remained from 40 to around 150 °C for both clay and hybrids. However, the weight loss decreased from 10.3 % to 6.7 % (monolayer Mtt-INH) and 3.4 % (multilayer Mtt-INH). This indicates a reduction in surface water following INH incorporation. A similar trend was observed after INH incorporation at pH 2. The second stage of the thermal decomposition process was narrower for the hybrids compared to Mtt with a corresponding decrease in weight loss. The third stage of decomposition was the most affected by the INH incorporation. In contrast to the other stages, the weight loss increased in proportion to the amount of INH adsorbed, as indicated by the adsorption results.

Table 4 shows the DTG peaks of Mtt and its hybrids. Based on TGA curves, the hybrids exhibited more peaks than Mtt itself. The peaks around 300, 380, and 580 °C can be attributed to INH degradation, as INH degradation typically shows peaks around 287 and 332 °C. The shift to higher temperatures in the decomposition of INH may indicate drug intercalation.

3.5. DSC

Fig. 5 shows the DSC curves of INH, Mtt, and their hybrids. The INH curve presents an endothermic peak around 175 °C, corresponding to the drug's melting point [40]. The influence of pH on clay is also evident from the difference between the curves at pH 7 (Mtt) and pH 2 (Mtt pH 2). The endothermic peaks in both curves are attributed to surface water loss. These peaks had a reduction after INH incorporation, due to the decrease in surface water, as observed in the TGA results. None of the hybrid curves exhibited the INH melting point peak, a finding also reported in other studies [40].

3.6. Release test

The release test mimicked the physiological pH conditions without enzymes to simulate the oral drug administration. In the first 2 h, the drug was exposed to pH 2, simulating the stomach environment; after, the pH was increased to 6.8 simulating the small intestine's first zone for 2 h, followed by 4 h at pH 7.4, simulating the small intestine. Fig. 6 shows the release profile of INH from its hybrids. As shown, the hybrid with drug concentration in monolayer adsorption (Mtt-INH (a)) did not release INH in the first 2 h of the experiment, at pH 2. The other hybrids with higher amounts of drug released it, especially the hybrid with INH deposited in multilayer on clay surface (Mtt-INH (b)). After the first 2 h, when the pH increased to 6.8, the release rate increased for all hybrids.

Table 5 presents the amount of INH released by the hybrids. The curves are shown in Fig. 6 indicate that, in percentage, the hybrids released nearly the same amount of INH after the 8 h of experiment. Since they incorporated different amounts of INH, as shown in Fig. 1, the hybrid Mtt-INH (c) presented the highest INH amount released at the end of the test, while the hybrid Mtt-INH (a) released the lowest amount. The hybrid Mtt-INH (b) released the highest amount of INH at pH 2, accounting for approximately 40 % of all INH released by this hybrid, compared to 0 % for hybrid Mtt-INH (a) and 16 % for hybrid Mtt-INH (c). Although hybrid Mtt-INH (a) released INH exclusively at pH 6.8 and above, the hybrid Mtt-INH (c) presented the highest release intestinal pH.

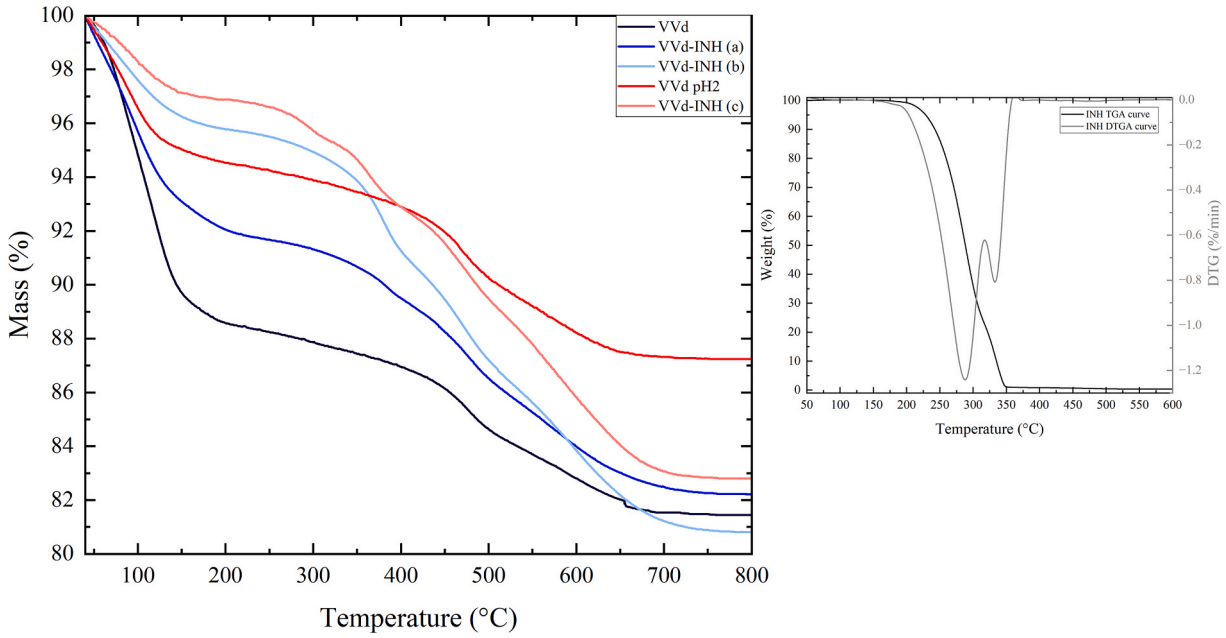

Fig. 4. TGA curves of Mtt and its hybrids.

Table 3
TGA weight loss description for Mtt and its hybrids separated by their stage of thermal degradation.

	Stage	1st stage	2nd stage			3rd stage		
Mtt	Temperature range (°C)	40–149	149–439	439–494	494–675	–	–	–
	Weight loss (%)	10.3	3.3	1.7	3.1	–	–	–
Mtt-INH (a)	Temperature range (°C)	40–144	144–349	349–433	433–497	497–668	–	–
	Weight loss (%)	6.7	2.6	1.9	2.2	3.8	–	–
Mtt-INH (b)	Temperature range (°C)	40–133	133–336	336–400	400–444	444–489	489–667	–
	Weight loss (%)	3.4	2.3	3.1	1.5	2.3	5.8	–
Mtt pH 2	Temperature range (°C)	40–132	132–415	415–502	502–643	–	–	–
	Weight loss (%)	4.7	2.6	2.5	2.6	–	–	–
Mtt-INH (c)	Temperature range (°C)	40–146	146–266	266–338	338–434	434–495	495–557	557–680
	Weight loss (%)	2.8	0.8	1.4	2.9	1.7	2.8	4.3

Table 4
Temperature and weight loss for INH, Mtt, and its hybrids.

DTG Peak		1	2	3	4	5
Mtt	Temperature (°C)	105	477	–	–	–
	Weight loss (%)	5.8	14.7	–	–	–
Mtt-INH (a)	Temperature (°C)	93	386	477	583	–
	Weight loss (%)	6.4	10.1	12.6	15.6	–
Mtt-INH (b)	Temperature (°C)	87	381	473	597	–
	Weight loss (%)	1.9	7.7	11.6	16.1	–
Mtt pH 2	Temperature (°C)	85	476	–	–	–
	Weight loss (%)	2.4	9.0	–	–	–
Mtt-INH (c)	Temperature (°C)	95	295	367	473	580
	Weight loss (%)	1.6	4.2	6.1	9.5	13.4

Table 6 presents the release fitting parameters for Mtt-INH hybrids using three mathematical models: zero-order, Higuchi, and Korsmeyer-Peppas. Higuchi's model provided the best fit for almost all the hybrids and their respective release media indicating that diffusion was the driving force of INH desorption from the clay [28]. Mtt-INH (b) and (c), at pH 7.4 and 2, respectively, Korsmeyer Peppas best fitted the release data. Their n parameters, which indicate the release mechanism, were 0.380 and 0.310, respectively, suggesting that the release was driven by Fickian diffusion [48]. Therefore, diffusion can be considered the driving force for INH release. The release of INH by Mtt/INH (c) closely followed the Zero-order model at pH 6.8 and 7.4 with R^2 higher than 0.936. This indicates that the drug release rate was independent of time and initial drug concentration.

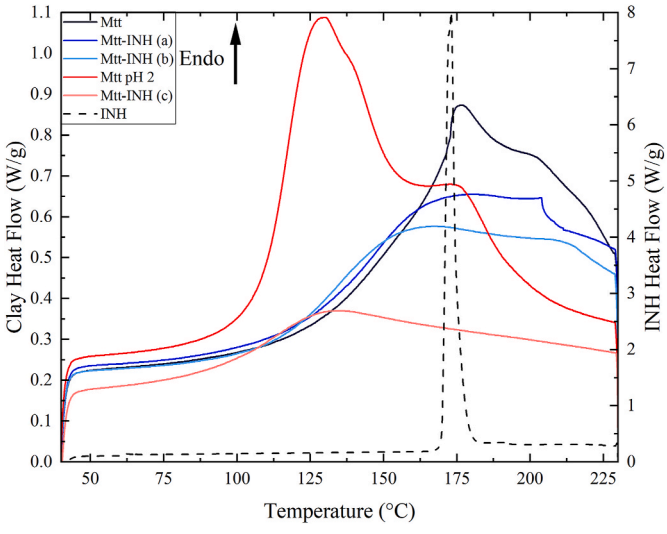

Fig. 5. DSC curves of INH, Mtt, and Mtt/INH hybrids.

Mtt-INH (c) and Mtt-INH (a) presented adsorption based on monolayer capacity, meaning the drug molecules were directly attached to the clay surface. In contrast, in Mtt-INH (b), most drug molecules were

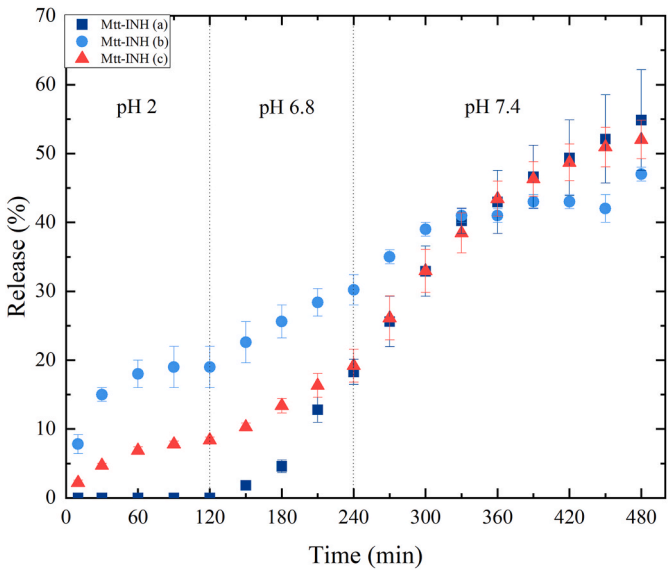

Fig. 6. Release profile of INH by Mtt/INH hybrids.

Table 5
Release the INH amount by time for the three hybrids Mtt/INH.

pH	Time (min)	Mtt-INH (a)		Mtt-INH (b)		Mtt-INH (c)	
		Release (mg/g)	Dev.	Release (mg/g)	Dev.	Release (mg/g)	Dev.
2	10	0.0	0.0	4.7	0.1	2.2	0.3
	30	0.0	0.0	9.0	0.1	4.6	0.3
	60	0.0	0.0	10.8	0.2	6.8	0.5
	90	0.0	0.0	11.4	0.3	7.7	0.4
	120	0.0	0.0	11.4	0.3	8.2	0.4
6.8	150	0.4	0.0	13.6	0.4	10.1	0.6
	180	0.9	0.0	15.4	0.4	13.1	1.0
	210	2.6	0.0	17.0	0.3	16.0	1.7
	240	3.7	0.1	18.1	0.4	18.8	2.3
7.4	270	5.1	0.2	21.0	0.2	25.6	3.1
	300	6.6	0.2	23.4	0.2	32.4	3.1
	330	8.0	0.1	24.6	0.2	37.8	2.9
	360	8.6	0.4	24.6	0.2	42.6	2.5
	390	9.3	0.4	25.8	0.3	45.5	2.5
	420	9.9	0.5	25.8	0.3	47.8	2.6
	450	10.4	0.7	25.2	0.5	50.0	2.8
	480	11.0	0.8	28.2	0.3	51.1	2.7

surrounded by other molecules. The stronger interaction between the clay and the drug in hybrids (a) and (c) likely contributes to a more controlled release profile, as these interactions help regulate the drug desorption over time. This behavior was reflected in their results fitting the zero-order release model, particularly for Mtt-INH (c), where the strong interaction between clay and drug was shown by the adsorption studies.

3.7. Cell viability

Fig. 7 shows the cell viability after 24 h of cell contact with the Mtt and Mtt-INH (c) extract. As shown, the pristine clay increased the cell viability of fibroblasts L929, while the Mtt-INH (c) presented a decrease of only 20 %, likely due to the presence of INH. Either clay or hybrid was not considered cytotoxic, as the average cell viability was above 80 %.

4. Discussion

The adsorption of INH by Mtt was studied by varying two parameters: the environment pH (2 and 7) and the initial drug concentration (Fig. 1). The pH of the environment influenced the shape of the adsorption curve, indicating that the interaction between Mtt and INH changed with pH [41,42].

At pH 7, the adsorption curve exhibited the L3 shape from the Giles system of isotherm classification. This type of curve suggests that the molecules were adsorbed flat on the clay surface [42]. The drug incorporation rate was higher at lower INH concentrations, as seen in the slope of the curve. When the adsorption curve at pH 7 reached point (a) (Fig. 8), the incorporation of INH reached a short plateau. This suggested that the solute molecules were not well oriented on the clay surface and had higher attraction for more solute molecules [42], probably by hydrogen bond interactions. These results were also observed by Carazo et al. (2018) and Souza et al. (2021) [36,40], indicating the achievement of a monolayer capacity. After reaching this point, the drug was deposited onto the drug molecules indicating a formation of multilayer drug deposition (point b).

At pH 2, the adsorption curve exhibited the shape H2, according to the classification by Giles et al. (1960) [42] For this kind of curve, the

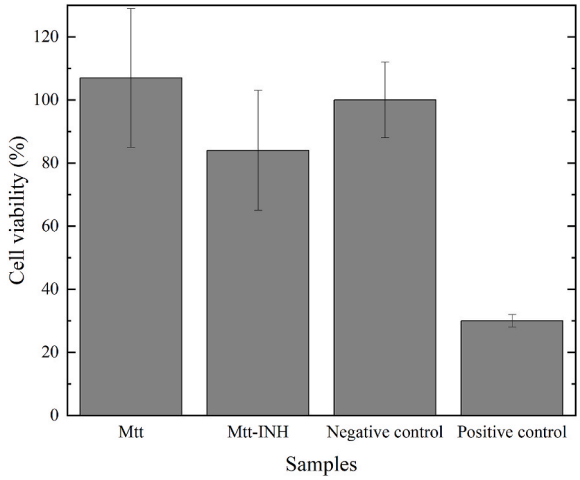

Fig. 7. Cell viability and standard deviation of cells incubated with the extracts of Mtt and Mtt-INH (c), with the negative and the positive control.

Table 6
Release fitting parameters of Mtt hybrids made at pH 2 and pH 7 in three different models: Zero-order, Higuchi, and Korsmeyer-Peppas.

Hybrid	pH	Zero order		Higuchi		Korsmeyer-Peppas		
		k_o	R^2	K_h	R^2	K_o	n	R^2
Mtt-INH (a)	2	–	–	–	–	–	–	–
	6.8	0.052	0.891	0.708	0.960	3.629	0.188	0.954
	7.4	0.115	0.951	2.259	0.966	1.897	0.530	0.965
Mtt-INH (b)	2	0.207	0.716	2.047	0.844	1.895	0.520	0.839
	6.8	0.135	0.700	1.923	0.994	1.056	0.613	0.993
	7.4	0.108	0.813	2.141	0.824	4.370	0.380	0.826
Mtt-INH (c)	2	0.084	0.893	0.814	0.969	1.860	0.310	0.986
	6.8	0.077	0.996	1.076	1.000	2.778	0.321	0.999
	7.4	0.113	0.936	2.219	0.954	1.894	0.527	0.953

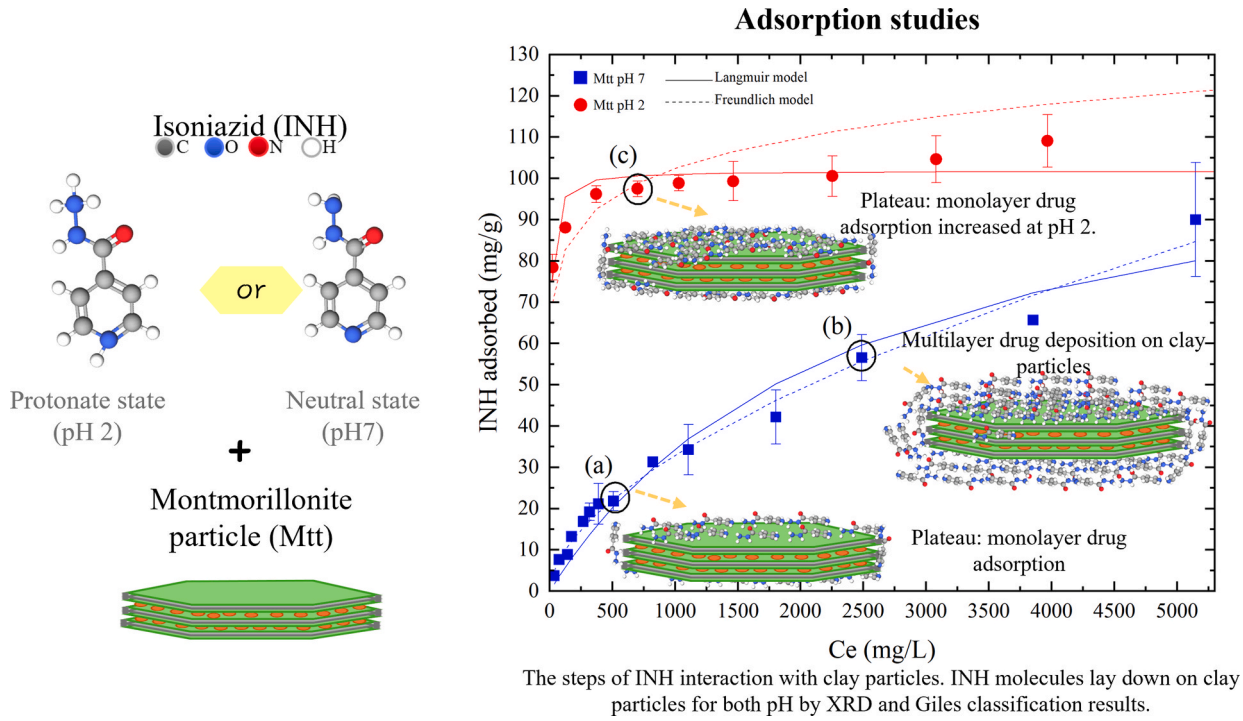

Fig. 8. Scheme of drug adsorption of INH by clay particle showing the morphology of clay-drug hybrids morphology and adsorption isotherm graph.

interaction between clay and the ionic drug is considered strong, with complete drug incorporation for concentrations lower than 800 mg/L. This occurs because, at pH 2, INH undergoes protonation at both endocyclic and exocyclic nitrogen sites. Since the Mtt surface charge is negative, the interaction between adsorbate and adsorbent is enhanced due to the stronger attachment to the negatively charged surface. Similar results were observed in other studies [27,28,36]. After reaching the monolayer adsorption capacity at point (c) in Fig. 8, the drug incorporation remained nearly constant at 100 mg/g. At this point, the drug molecules were immediately attached to the clay surface. The positive interaction from the drug layers repelled other positive molecules regardless of the drug concentration in the solution, which hindered further drug incorporation, resulting in a long plateau [41,42]. Furthermore, the curves obtained at both pHs best fitted the Freundlich model suggesting that heterogeneous adsorption occurred with INH interacting with the negatively charged faces of the lamella and varying interactions between the drug and clay edges [44].

All FTIR spectra of the Mtt-INH hybrid were similar to pristine Mtt (Fig. 2). This similarity occurred because the amount of clay was higher than the drug amount in the hybrid, as observed in previous studies [27–31,35,40]. The hybrid with a small amount of INH, Mtt-INH (a) exhibited only one band from INH, around 1437 cm^{-1}. This band is attributed to the INH ring stretching vibration [35,40]. For the hybrids (b) and (c), the appearance of bands from 1600 to 1400 cm^{-1} is related to INH ring vibration modes. The increase of the 754 cm^{-1} band in the hybrids was due to the presence of C-H bonds in the INH ring [35]. For the hybrid Mtt-INH (c), in addition to the bands seen in Mtt-INH (b), the appearance of bands at 1692 and 1248 cm^{-1} was observed. The band around 1692 cm^{-1} was a shift of the 1668 cm^{-1} band of the INH carbonyl group (C=O). Previous studies have shown that this shift is caused by the change in oxygen vibration of the carbonyl group vibration due to hydrogen bond interaction [30]. The band around 1632 cm^{-1} in the clay spectrum is attributed to the OH stretching vibration of the water molecules adsorbed on the clay surface [31,45,49]. Its downward in the hybrid spectrum can be related to the hydrogen bonds with INH. This result was also observed in the hybrid obtained by Carazo et al. (2018) [40]. For MTT-INH (c), the upward shift of the Si-O stretching band from 998 to 1003 cm^{-1} is associated with the Si-O stretching mode of aluminosilicates, which was affected by the orientation of the clay platelets [35] after the positively charged drug incorporation. As proposed in previous studies, the FTIR results suggest an interaction between the clay and the INH carboxyl, hydrazine, and pyridine groups [35,40].

XRD curves, Fig. 3, showed a decrease in the interlayer spacing, which was also observed in other studies [44,50]. This decrease is attributed to the reduction of interlayer water molecules in the clay due to drug incorporation [17,18,44]. These findings align with the results obtained from TGA analysis. In all adsorption systems, there is a competition between the solute (INH) and the solvent (water) for adsorption [41]. The reduction of water molecules within the clay structure can be explained by the greater affinity of INH for the clay surface than water molecules. Previous studies have suggested that the interaction between the drug and clay may occur at various sites within the clay not limited to the interlayer space. These interactions include the binding of the positively charged drug to the negatively charged surfaces of the clay lamellae [11,15,18].

Fig. 4 presents the TGA curves for INH, Mtt, and their hybrids. Generally, the TGA curves of clays and their hybrids can be divided into three stages. The first stage, characterized by an abrupt weight loss, corresponds to the loss of surface water, which decreases as the amount of INH incorporated into the clay increases. The second stage involves a slower weight loss rate due to the loss of inner water molecules. The third stage is associated with the dihydroxylation process and the degradation of INH. All three decomposition stages of Mtt were affected by the presence of the drug. The reduction of surface water following INH incorporation in clays supports the results of the adsorption test, confirming that the drug-clay interaction is stronger than the water-clay interaction. For the hybrid with the highest INH content, Mtt-INH (c), the second degradation stage occurred over the shortest temperature range (from 146 to 266 °C). This suggests that the presence of INH replaces the inner water molecules typically attached to clay structure pore structures, corroborating the XRD results. The emergence of new peaks in DTG analysis confirmed INH degradation of INH during the third stage of decomposition. The degradation temperature of INH

increased after clay incorporation, indicating that the drug was well-bound to and protected by clay. These results align with the DSC analysis, where the melting peak of INH was absent in all hybrids studied. This confirms the formation of a high-affinity hybrid rather than a simple physical mixture of clay and drug as suggested by the work of Carazo et al. (2018) [40].

The pH-dependence interaction between clay and INH also influenced the release profile. Mimicking the release of oral administration, drug release was reduced at acidic pH levels, as shown in Fig. 6. At pH 2, the release for hybrids Mtt-INH (b) and (c) quickly reached a plateau within the first 60 min, whereas no detectable amount of INH was released from hybrid Mtt-INH (a). Hybrid Mtt-INH (a), prepared with INH at its monolayer capacity at pH 7, exhibited no release pH 2 because the protonated INH molecules were more strongly bound to the negatively charged Mtt surface. For Mtt-INH (b), part of the INH molecules was not in contact with the Mtt surface, as some drug molecules were deposited on top of existing INH layers. In this case, the protonated INH could not fully interact with the Mtt surface leading to partial release. For Mtt-INH (c) additional phenomena were observed. Adsorption at pH 2 occurred under equilibrium conditions, where part of the drug was adsorbed onto the clay surface while the remainder remained in the surrounding medium. When the hybrid was subsequently exposed to the same pH, a portion of the drug was released to restore the equilibrium. At pH 6.8 and 7.4, the hybrids exhibited an increased drug release rate. Although the percentage of drug released was similar across all hybrids, Mtt-INH (c) released a larger absolute amount of INH. Furthermore, Mtt-INH (c) was the only hybrid to fit in the Zero-order release model. This finding is significant is important as it suggests that the drug can be released at a constant rate throughout the release process [28]. All hybrids presented an incomplete release profile, similar results were observed in other studies [28,33,36,44].

The hybrid Mtt-INH (c) exhibited the highest level of INH incorporation, approximately 100 mg/g, and the highest amount of drug released. Notably, one of the most common dosages of INH pills is 100 mg, with a maximum of 300 mg, suggesting that this hybrid could be suitable for such application. Also, regarding the clay intaking, these results align with previous studies reporting a 1.5 g/daily Mtt dose in children [51], and a safe 40 mg/kg/daily dose of Mtt in adult rats [52]. Furthermore, cytotoxic tests demonstrated that neither pristine clay nor clay-INH were cytotoxic to fibroblasts L929 cells. These findings indicate that this hybrid has potential as a controlled release system for INH.

5. Conclusions

Our study provided novel insights into the role of electrostatic interactions in drug-clay systems, supported by structural, morphological, and thermodynamic characterizations. Previous studies have highlighted the significance of pore volume in neutral drug adsorption. However, our study demonstrates, for the first time, that drug incorporation mechanisms at pH 2 and pH 7 differ fundamentally, directly influencing the drug release profile.

As was shown in other studies, at pH 7, where INH remains in its neutral state, drug adsorption occurs in two distinct phases: monolayer adsorption (INH directly binds to the clay surface, reaching monolayer saturation of 20 mg/g) and multilayer deposition (beyond the monolayer, additional drug molecules stack onto each other, incorporating up to 110 mg/g). While multilayer adsorption increases drug loading, it results in weaker drug-clay interactions, leading to burst release, with ~20 % of the drug released in acidic conditions. In contrast, monolayer adsorption, characterized by stronger surface interactions, prevents premature release in the gastric environment, a crucial factor for oral drug formulations.

At pH 2, where INH is in its protonated state, adsorption is primarily driven by electrostatic attraction between the positively charged drug and negatively charged clay. However, strong electrostatic repulsion between protonated drug molecules limits adsorption to monolayer capacity of 100 mg/g, preventing multilayer incorporation. As a result, drug release at acidic pH is significantly lower (~8 %), and in higher pH environments (6.8 and 7.4), it presented zero-order release profile, which is often desirable for sustained drug delivery applications.

FTIR analysis revealed that INH chemical groups play a key role in the adsorption, by interacting with clay functional groups such as Si-O and O-H. TGA and DSC results indicated that clay particles provide thermal protection to the drug, preventing its transformation and decomposition.

These findings elucidate the fundamental relationship between drug incorporation mechanisms and release behavior, providing a reference background for future studies on neutral and cationic drug adsorption in clay-based systems. The results here can guide the design of optimized clay-based carriers for controlled drug release, particularly for oral administration, where preventing premature drug release in the stomach may be critical. Besides that, the findings of this study suggest that Brazilian natural clay, which exhibited no cytotoxicity, could serve as a cost-effective alternative for tuberculosis treatment.

Likewise, the adsorption process, which occurs in water by dispersing montmorillonite (Mtt) into an INH solution under stirring at room temperature, is highly scalable. This method aligns well with conventional reactor designs commonly used in pharmaceutical manufacturing. However, scaling up may introduce challenges related to heat transfer and material flow differences compared to the laboratory scale. These factors could influence adsorption efficiency and yield, but process optimization, such as adjusting mixing conditions and residence time, can mitigate these effects and ensure reproducibility at an industrial scale.

Funding sources

This work was supported by the CNPq (*Conselho Nacional de Desenvolvimento Científico e Tecnológico*), grant number 141859/2020–2; CAPES (*Coordenação de Aperfeiçoamento de Pessoal de Nível Superior*), grant number 88887.694,663/2022–00; FAPESP (*Fundação de Amparo à Pesquisa do Estado de São Paulo*), grant number 2019/01231–2 and 2022/00662–2; and NSERC (Natural Sciences and Engineering Research Council of Canada), grant number ALLRP 573019–22 as well Canadian Research Chair Tier 1.

In this work, the authors used ChatGPT to refine and improve the clarity and grammar of certain sentences. However, it was solely employed for language enhancement, without contributing to creating any scientific content or ideas. After using this tool/service, the authors reviewed and edited the content as needed and took full responsibility for the publication's content.

CRediT authorship contribution statement

Jessica de Carvalho Arjona: Conceptualization, Data curation, Formal analysis, Investigation, Methodology, Software, Validation, Visualization, Writing – original draft, Writing – review & editing. **Carina Ulsen:** Conceptualization, Data curation, Formal analysis, Methodology, Resources, Software, Validation, Writing – review & editing. **Dayane Tada:** Data curation, Formal analysis, Investigation, Methodology, Resources, Validation, Writing – review & editing. **Francisco Rolando Valenzuela Diaz:** Conceptualization, Data curation, Funding acquisition, Investigation, Methodology, Project administration, Resources, Supervision, Validation, Visualization, Writing – review & editing. **Nicole Raymonde Demarquette:** Conceptualization, Investigation, Project administration, Resources, Supervision, Validation, Visualization, Writing – original draft, Writing – review & editing.

Declaration of competing interest

The authors declare that they have no known competing financial interests or personal relationships that could have appeared to influence the work reported in this paper.

Acknowledgment

The authors acknowledge and express their gratitude for the infrastructural assistance provided by LIPEC-PolymerETS (*Laboratoire d'ingénierie des polymères et composites* at ÉTS) and STEPPE (*Station Expérimentale des Procédés Pilotes en Environnement* at ÉTS). They also wish to thank Research Associate Dr. Mazen Samara for the writing assistance, Dr. Maria das Graças Silva-Valenzuela for her expertise and assistance throughout this study, and the undergraduate student Ms. Colyne Jacques for conducting some adsorption and release tests.

Data availability

Data will be made available on request.

References

[1] M.I. Carretero, Clay minerals and their beneficial effects upon human health. A review, Appl. Clay Sci. 21 (2002) 155–163, https://doi.org/10.1016/S0140-6736(00)90347-7.
[2] C. Aguzzi, P. Cerezo, C. Viseras, C. Caramella, Use of Clays as Drug Delivery Systems : Possibilities and Limitations, 36, 2007, pp. 22–36, https://doi.org/10.1016/j.clay.2006.06.015.
[3] S.F. Hulbert, S. Carolina, L.S. Bowman, S. Carolina, History of ceramic orthopedic implants, Mater. Res. Bull. 7 (1972) 1239–1246.
[4] C. Del Hoyo, Layered Double Hydroxides and Human Health : an Overview, 36, 2007, pp. 103–121, https://doi.org/10.1016/j.clay.2006.06.010.
[5] F. Bergaya, B. Theng, G. Lagaly, Handbook of clay science, Elsevier, in: Handbook of Clay Science, fourth ed., Elsevier, San Diego - California, 2005.
[6] G. Lagaly, M.F. Gonzalez, A. Weiss, Problems in layer-charge determination of montmorillonites, Clay Miner. 11 (1976) 173–187.
[7] G. Lagaly, General introduction : clays , clay minerals, Clay Sci. 1 (2006), https://doi.org/10.1016/S1572-4352(05)01001-9.
[8] M.A. Djebbi, S. Boubakri, Z. Bouaziz, M.S. Elayachi, P. Namour, N. Jaffrezic-Renault, A. Ben Haj Amara, Extended-release of chlorpromazine intercalated into montmorillonite clays, Microporous Mesoporous Mater. 267 (2018) 43–52, https://doi.org/10.1016/j.micromeso.2018.03.017.
[9] M.D. Alqahtani, M.N. Bin Jumah, A. Al-Hashimi, A.A. Allam, M.R. Abukhadra, S. Bellucci, Synthesis and characterization of methoxy-exfoliated montmorillonite nanosheets as potential carriers of 5-fluorouracil drug with enhanced loading, release, and cytotoxicity properties, Molecules 28 (2023), https://doi.org/10.3390/molecules28155895.
[10] I. Calabrese, G. Cavallaro, C. Scialabba, M. Licciardi, M. Merli, L. Sciascia, M. L. Turco Liveri, Montmorillonite nanodevices for the colon metronidazole delivery, Int. J. Pharm. 457 (2013) 224–236, https://doi.org/10.1016/j.ijpharm.2013.09.017.
[11] B.D. Kevadiya, T.A. Patel, D.D. Jhala, R.P. Thumbar, H. Brahmbhatt, M.P. Pandya, S. Rajkumar, P.K. Jena, G.V. Joshi, P.K. Gadhia, C.B. Tripathi, H.C. Bajaj, Layered inorganic nanocomposites: a promising carrier for 5-fluorouracil (5-FU), Eur. J. Pharm. Biopharm. 81 (2012) 91–101, https://doi.org/10.1016/j.ejpb.2012.01.004.
[12] H. Çiftçi, M.D. Arpa, İ.M. Gülaçar, L. Özcan, B. Ersoy, Development and evaluation of mesoporous montmorillonite/magnetite nanocomposites loaded with 5-Fluorouracil, Microporous Mesoporous Mater. 303 (2020), https://doi.org/10.1016/j.micromeso.2020.110253.
[13] L. Sciascia, I. Calabrese, G. Cavallaro, M. Merli, C. Scialabba, M.L.T. Liveri, Modified montmorillonite as drug delivery agent for enhancing antibiotic therapy, Minerals 11 (2021), https://doi.org/10.3390/min11121315.
[14] B. Gulen, P. Demircivi, Synthesis and characterization of montmorillonite/ciprofloxacin/TiO2 porous structure for controlled drug release of ciprofloxacin tablet with oral administration, Appl. Clay Sci. 197 (2020), https://doi.org/10.1016/j.clay.2020.105768.
[15] S.A. Martín, I. Pérez, A. Rivera, Hosting of the antibiotic Vancomycin by bentonite: characterization and slow release study, Appl. Clay Sci. 202 (2021), https://doi.org/10.1016/j.clay.2020.105965.
[16] M. Kaur, M. Datta, Diclofenac Sodium Adsorption onto Montmorillonite: Adsorption Equilibrium Studies and Drug Release Kinetics, n.d.
[17] I. Calabrese, G. Gelardi, M. Merli, M.L.T. Liveri, L. Sciascia, Clay-biosurfactant materials as functional drug delivery systems: slowing down effect in the in vitro release of cinnamic acid, Appl. Clay Sci. 135 (2017) 567–574, https://doi.org/10.1016/j.clay.2016.10.039.
[18] G.R.S. Cavalcanti, M.G. Fonseca, E.C. da Silva Filho, M. Jaber, Thiabendazole/bentonites hybrids as controlled release systems, Colloids Surf. B Biointerfaces 176 (2019) 249–255, https://doi.org/10.1016/j.colsurfb.2018.12.030.
[19] G.V. Joshi, H.A. Patel, B.D. Kevadiya, H.C. Bajaj, Montmorillonite intercalated with vitamin B1 as drug carrier, Appl. Clay Sci. 45 (2009) 248–253, https://doi.org/10.1016/j.clay.2009.06.001.
[20] G.V. Joshi, B.D. Kevadiya, H.C. Bajaj, Design and evaluation of controlled drug delivery system of buspirone using inorganic layered clay mineral, Microporous Mesoporous Mater. 132 (2010) 526–530, https://doi.org/10.1016/j.micromeso.2010.04.003.
[21] G.V. Joshi, B.D. Kevadiya, H.A. Patel, H.C. Bajaj, R.V. Jasra, Montmorillonite as a drug delivery system: intercalation and in vitro release of timolol maleate, Int. J. Pharm. 374 (2009) 53–57, https://doi.org/10.1016/j.ijpharm.2009.03.004.
[22] M. Gajendiran, H. Jo, K. Kim, S. Balasubramanian, In vitro controlled release of tuberculosis drugs by amphiphilic branched copolymer nanoparticles, J. Ind. Eng. Chem. 77 (2019) 181–188, https://doi.org/10.1016/j.jiec.2019.04.033.
[23] N. Genina, J.P. Boetker, S. Colombo, N. Harmankaya, J. Rantanen, A. Bohr, Anti-tuberculosis drug combination for controlled oral delivery using 3D printed compartmental dosage forms: from drug product design to in vivo testing, J. Contr. Release 268 (2017) 40–48, https://doi.org/10.1016/j.jconrel.2017.10.003.
[24] M.A. Altamimi, A. Hussain, S.S. Imam, S. Alshehri, S.K. Singh, T.J. Webster, Transdermal delivery of isoniazid loaded elastic liposomes to control cutaneous and systemic tuberculosis, J. Drug Deliv. Sci. Technol. 59 (2020) 101848, https://doi.org/10.1016/j.jddst.2020.101848.
[25] P.M. Oliveira, B.N. Matos, P.A.T. Pereira, T. Gratieri, L.H. Faccioli, M.S.S. Cunha-Filho, G.M. Gelfuso, Microparticles prepared with 50–190 kDa chitosan as promising non-toxic carriers for pulmonary delivery of isoniazid, Carbohydr. Polym. 174 (2017) 421–431, https://doi.org/10.1016/j.carbpol.2017.06.090.
[26] R.C. Marengo, L.N. Mengatto, M.L. Olivares, C.L.A. Berli, Microfluidics-based encapsulation of isoniazid in egg white/carrageenan microparticles for sustained release, Food Hydrocolloids for Health 1 (2021) 100041, https://doi.org/10.1016/j.fhfh.2021.100041.
[27] J.M.F. de Almeida, E. Damasceno Júnior, L.M. Verrísimo, N.S. Fernandes, pH-Dependent release system of isoniazid carried on nanoparticles of silica obtained from expanded perlite, Appl. Surf. Sci. 489 (2019) 297–312, https://doi.org/10.1016/j.apsusc.2019.05.317.
[28] E. Damasceno Junior, J.M.F. de Almeida, I. do N. Silva, M.L. Moreira de Assis, L. M. dos Santos, E.F. Dias, V.E. Bezerra Aragão, L.M. Veríssimo, N.S. Fernandes, D. R. da Silva, E.D. Junior, J. Mayara, F. De Almeida, N. Silva, M. Lizandra, M. De Assis, L. Maciel, E.F. Dias, V. Eduardo, B. Aragão, L.M. Veríssimo, N.S. Fernandes, D. Ribeiro, pH-responsive release system of isoniazid using palygorskite as a nanocarrier, J. Drug Deliv. Sci. Technol. 55 (2019) 101399, https://doi.org/10.1016/j.jddst.2019.101399.
[29] E. Carazo, A. Borrego-Sánchez, F. García-Villén, R. Sánchez-Espejo, C. Viseras, P. Cerezo, C. Aguzzi, Adsorption and characterization of palygorskite-isoniazid nanohybrids, Appl. Clay Sci. 160 (2018) 180–185, https://doi.org/10.1016/j.clay.2017.12.027.
[30] S. Akyuz, T. Akyuz, E. Akalin, Adsorption of isoniazid onto sepiolite-palygorskite group of clays: an IR study, Spectrochim. Acta Mol. Biomol. Spectrosc. 75 (2010) 1304–1307, https://doi.org/10.1016/j.saa.2009.12.069.
[31] E. Carazo, A. Borrego-Sánchez, F. García-Villén, R. Sánchez-Espejo, C. Aguzzi, C. Viseras, C.I. Sainz-Díaz, P. Cerezo, Assessment of halloysite nanotubes as vehicles of isoniazid, Colloids Surf. B Biointerfaces 160 (2017) 337–344, https://doi.org/10.1016/j.colsurfb.2017.09.036.
[32] E. Carazo, G. Sandri, P. Cerezo, C. Lanni, F. Ferrari, C. Bonferoni, C. Viseras, C. Aguzzi, Halloysite nanotubes as tools to improve the actual challenge of fixed doses combinations in tuberculosis treatment, J. Biomed. Mater. Res. 107 (2019) 1513–1521, https://doi.org/10.1002/jbm.a.36664.
[33] B. Saifullah, M.E. El Zowalaty, P. Arulselvan, S. Fakurazi, T.J. Webster, B. M. Geilich, M.Z. Hussein, Synthesis, characterization, and efficacy of antituberculosis isoniazid zinc aluminum-layered double hydroxide based nanocomposites, Int. J. Nanomed. 11 (2016) 3225–3237, https://doi.org/10.2147/IJN.S102406.
[34] E.A. Banu, L.D. Duceac, G. Mitrea, M.I. Ciuhodaru, D.L. Ichim, I.M. Ciomaga, R.E. B. Goroftei, M. Constantin, G. Baciu, Synthesis and physico-chemical characterization of nanohybrid materials based on isonicotinic acid hydrazide, Mater. Plast. 56 (2019). http://www.revmaterialeplastice.ro.
[35] S. Akyuz, T. Akyuz, FT-IR and FT-Raman spectroscopic studies of adsorption of isoniazid by montmorillonite and saponite, Vib. Spectrosc. 48 (2008) 229–232, https://doi.org/10.1016/j.vibspec.2008.02.019.
[36] I.M.S. Souza, A. Borrego-Sánchez, C.I. Sainz-Díaz, C. Viseras, S.B.C. Pergher, Study of Faujasite zeolite as a modified delivery carrier for isoniazid, Mater. Sci. Eng. C 118 (2021) 12, https://doi.org/10.1016/j.msec.2020.111365.
[37] I.M.S. Souza, C.I. Sainz-Díaz, C. Viseras, S.B.C. Pergher, Adsorption capacity evaluation of zeolites as carrier of isoniazid, Microporous Mesoporous Mater. 292 (2020), https://doi.org/10.1016/j.micromeso.2019.109733.
[38] J. de Carvalho Arjona, C. Ulsen, F.R. Valenzuela-Diaz, N.R. Demarquette, Influence of smectite clays' pores volume on isoniazid adsorption and release, Appl. Clay Sci. 252 (2024), https://doi.org/10.1016/j.clay.2024.107341.
[39] E. Çalışkan Salihi, Z. Gündüz, A.S. Baştuğ, E.Ç. Salihi, Z. Gündüz, A.S. Baştuğ, Fast retention of isoniazid on organobentonite prepared using green chemistry approach: contribution of the π interactions, Separ. Sci. Technol. 54 (2019) 2695–2705, https://doi.org/10.1080/01496395.2018.1543324.
[40] E. Carazo, A. Borrego-Sánchez, R. Sánchez-Espejo, F. García-Villén, P. Cerezo, C. Aguzzi, C. Viseras, Kinetic and thermodynamic assessment on isoniazid/montmorillonite adsorption, Appl. Clay Sci. 165 (2018) 82–90, https://doi.org/10.1016/j.clay.2018.08.009.
[41] C.H. Giles, D. Smith, A general treatment and classification of the solute adsorption isotherm, Bronx County Hist. Soc. J. 47 (1974) 755–765, https://doi.org/10.1007/s41193-016-0111-5.
[42] C.H. Giles, T.H. MacEwan, S.N. Nakhwa, D. Smith, Studies in adsorption. Part XI. A system of classification of solution adsorption isotherms, and its use in diagnosis of adsorption mechanisms and in measurement of specific surface areas of solids, J. Chem. Soc. (1960) 3973–3993, https://doi.org/10.1039/jr9600003973.
[43] M. das G. Silva-Valenzuela, M.M. Chambi-Peralta, I.J. Sayeg, F.M. de Souza Carvalho, S.H. Wang, F.R. Valenzuela-Díaz, Enrichment of clay from Vitoria da

Conquista (Brazil) for applications in cosmetics, Appl. Clay Sci. 155 (2018) 111–119, https://doi.org/10.1016/j.clay.2018.01.011.
[44] I. Calabrese, G. Cavallaro, C. Scialabba, M. Licciardi, M. Merli, L. Sciascia, M. L. Turco Liveri, Montmorillonite nanodevices for the colon metronidazole delivery, Int. J. Pharm. 457 (2013) 224–236, https://doi.org/10.1016/j.ijpharm.2013.09.017.
[45] M.G. Bekaroğlu, F. Nurili, S. İşçi, Montmorillonite as imaging and drug delivery agent for cancer therapy, Appl. Clay Sci. 162 (2018) 469–477, https://doi.org/10.1016/j.clay.2018.06.039.
[46] L.B. de Paiva, A.R. Morales, F.R. Valenzuela Díaz, Organoclays: properties, preparation and applications, Appl. Clay Sci. 42 (2008) 8–24, https://doi.org/10.1016/j.clay.2008.02.006.
[47] S.L. Swartzen-Allen, E. Matijevic, Surface and colloid chemistry of clays, Chem. Rev. 74 (1974) 385–400.
[48] R. Atif, T. Salah Eldeen, L. Ahmed, I. Yahya, A. Omara, M. Eltayeb, Study the using of nanoparticles as drug delivery system based on mathematical models for controlled release, International Journal of Latest Technology in Engineering VIII (2019) 52–56. www.ijltemas.
[49] F.G. Alabarse, R.V. Conceição, N.M. Balzaretti, F. Schenato, A.M. Xavier, In-situ FTIR analyses of bentonite under high-pressure, Appl. Clay Sci. 51 (2011) 202–208, https://doi.org/10.1016/j.clay.2010.11.017.
[50] L. Bromberg, C.M. Straut, A. Centrone, E. Wilusz, T.A. Hatton, Montmorillonite functionalized with pralidoxime as a material for chemical protection against organophosphorous compounds, ACS Appl. Mater. Interfaces 3 (2011) 1479–1484, https://doi.org/10.1021/am200041e.
[51] N.J. Mitchell, J. Kumi, M. Aleser, S.E. Elmore, K.A. Rychlik, K.E. Zychowski, A. A. Romoser, T.D. Phillips, N.-A. Ankrah, Short-term safety and efficacy of calcium montmorillonite clay (UPSN) in children, Am. Soc. Trop. Med. Hygiene 91 (2014) 777–785. https://doi.org/10.4269/ajtmh.14-0093.
[52] S. Maisanaba, S. Pichardo, M. Puerto, D. Gutiérrez-Praena, A.M. Cameán, A. Jos, Toxicological evaluation of clay minerals and derived nanocomposites: a review, Environ. Res. 138 (2015) 233–254. https://doi.org/10.1016/j.envres.2014.12.024.